Eur Biophys J (2001) 30: 319–329
DOI 10.1007/s002490100152

ARTICLE

S.-H. Chong · Y. Joti · A. Kidera · N. Go
A. Ostermann · A. Gassmann · F. Parak

Dynamical transition of myoglobin in a crystal: comparative studies of X-ray crystallography and Mössbauer spectroscopy

Received: 4 January 2001 / Revised version: 8 March 2001 / Accepted: 8 March 2001 / Published online: 17 May 2001

Abstract The crystallographic normal mode refinements of myoglobin at a wide range of temperature from 40 K to 300 K were carried out to study the temperature dependence of the internal atomic fluctuations. The refinement method decomposes the mean square displacement from the average position, $\langle \Delta r^2 \rangle$, into the contributions from the internal degrees of freedom and those from the external degrees of freedom. The internal displacements show linear temperature dependence as $\langle \Delta r^2 \rangle = \alpha T + \beta$, throughout the temperature range measured here, and exhibit no obvious change in the slope α at the dynamical transition temperature (T_c = ca. 180 K). The slope α is practically the same as the value predicted theoretically by normal mode analysis. Such linear dependence is considered to be due to the following reason. The crystallographic Debye-Waller factor represents the static distribution caused by convolution of temperature-dependent normal mode motions and a temperature-independent set of the conformational substates. In contrast, Mössbauer absorption spectroscopy shows a clear increase in the gradient α at T_c. This difference from X-ray diffraction originates from the incoherent nature of the Mössbauer effect together with its high-energy resolution, which yields the self-correlation, and the temporal behavior of individual Fe atoms in the myoglobin crystal.

A. Ostermann · A. Gassmann · F. Parak (✉)
Physik-Department E17,
Technische Universität München,
85747 Garching, Germany
E-mail: fritz.parak@ph.tum.de

S.-H. Chong · Y. Joti · A. Kidera · N. Go
Department of Chemistry,
Graduate School of Science,
Kyoto University, Sakyo-ku,
Kyoto 606, Japan

Keywords Mössbauer spectroscopy · Myoglobin · Protein dynamics · X-ray crystallography

Introduction

The X-ray structure determination of a protein is of fundamental importance for understanding of the protein function. However, in many cases the atomic coordinates are not sufficient; dynamic properties are essential. A classical example is found in myoglobin, where the molecule stores one oxygen molecule at the iron of the heme group within the molecule. Although the X-ray structure of myoglobin is known in detail, one cannot find a channel allowing the oxygen molecule to pass into its binding site within the heme pocket. Structure fluctuations opening the entrance channel are necessary.

For many years, structural fluctuations of proteins have been studied by many physical methods. X-ray structure analysis by itself reveals protein dynamics; this information is contained in the Debye-Waller factor. While the coordinates of the molecule obtained from X-ray data represent the average values over all molecules within a crystal, the individual Debye-Waller factor for each atom yields the mean square displacement, $\langle \Delta r^2 \rangle^X$, which represent the width of a Gaussian distribution around the average coordinates. However, the conventional X-ray scattering has no time resolution. The ensemble average does not depend on the time which an atom needs to be displaced from its average position. Static displacement and displacements on any time scale are reflected in the same way.

There are several ways to overcome this difficulty. First of all, the X-ray structure can be determined as a function of temperature. A reduction of the mean square displacement with decreasing temperature should indicate dynamic effects, which can be frozen out at low temperatures. Another help is the use of spectroscopic methods, which have a built-in time dependence. Mössbauer spectroscopy on the isotope ^{57}Fe has proved

to be a good tool to investigate protein dynamics of iron-containing proteins. In analogy to the Debye-Waller factor of the X-ray analysis, the Lamb Mössbauer factor gives a mean square displacement of the iron, $\langle \Delta r^2 \rangle^{\gamma}$. However, here only dynamic displacements contribute, occurring on a time scale faster than the nuclei decay time of the 14.4 keV Mössbauer transition. Therefore, X-ray diffraction and Mössbauer spectroscopy on myoglobin can be used in a complementary way to obtain more detailed information on protein dynamics over a large temperature range (Parak and Formanek 1971; Parak et al. 1987).

In the study of temperature dependence of protein dynamics, a dynamical transition similar to the glass transition should be one of the important issues to be focused. Although such a transition may not be so well defined in proteins than in glasses (Green et al. 1994), it is characterized by an abrupt increase in atomic fluctuations above ~180 K. This phenomenon has been detected by various spectroscopic techniques, such as Mössbauer spectroscopy (Parak and Formanek 1971; Parak et al. 1982), Rayleigh scattering of Mössbauer radiation (Krupyanskii et al. 1982; Nienhaus and Parak 1986), and neutron incoherent scattering (Doster et al. 1989; Ferrand et al. 1993), as well as by X-ray structure analysis of myoglobin after flash photolysis of CO (Ostermann et al. 2000). From these experimental studies, the following characteristic features of protein dynamics were found (Parak and Knapp 1984). Below the dynamical transition temperature ($T_c \approx 180$ K), a protein molecule is trapped in one of the conformational substates, and undergoes almost harmonic motions within a basin of the potential surface. Thus, the temperature dependence of the mean square displacements is linear, and its gradient is close to one as predicted by a normal mode analysis. Above the dynamical transition temperature the gradient suddenly increases, owing to the onset of jumping among different conformational substates. It has been argued that such anharmonic motions are crucial for a protein function (Rasmussen et al. 1992). The purpose of this study is to clarify how this picture of Mössbauer spectroscopy fits with the results of the normal mode refinement.

In this paper, we will show the result of an elaborate data analysis, the normal mode refinement (NM-REF) (Kidera and Go 1992; Kidera et al. 1992), of X-ray diffraction data over a wide temperature range (Parak et al. 1987), and compare the result with data from Mössbauer spectroscopy. First, we review the principles of X-ray diffraction and Mössbauer absorption spectroscopy to clarify the difference in the dynamics information derived from the two methods. Second, the theory of the normal mode refinement is explained in terms of the conformational substates. Then, the temperature dependence of the mean square displacements derived from the normal mode refinement is compared with that of Mössbauer spectroscopy to reveal the detailed information about the dynamics of myoglobin in a crystal. Preliminary results have already been given by Parak et al. (1999).

Difference in dynamics obtained from X-ray diffraction and Mössbauer absorption spectroscopy

When we try to understand the experimental data, we should first consider the fundamental difference between the dynamics information obtained from X-ray diffraction and Mössbauer absorption spectroscopy. As pointed out by Mössbauer (1987), the difference originates from the coherent nature of X-ray diffraction and the incoherent nature of Mössbauer radiation, together with a different energy resolution. Here, we will briefly review the principles of the two experimental methods.

Because the X-ray scattering process is of a coherent nature, the double differential cross section is described by:

$$\frac{\mathrm{d}^2\sigma}{\mathrm{d}\Omega \mathrm{d}\omega} \propto S[\mathbf{k},\omega] = \frac{1}{2\pi}\int_{-\infty}^{\infty} \sum_i \sum_j f_i^*[\mathbf{k}] f_j[\mathbf{k}] \langle \mathrm{e}^{i\mathbf{k}\mathbf{r}_i[t]} \mathrm{e}^{-i\mathbf{k}\mathbf{r}_j[0]} \rangle \mathrm{e}^{-i\omega t} \mathrm{d}t \qquad (1)$$

where $f_i[\boldsymbol{k}]$ is the atomic scattering factor for atom i, $\boldsymbol{r}_i[t]$ is the position vector of atom i at time t, and the angle bracket gives the (i,j) component of the intermediate scattering function. The scattered X-ray beam is described as a function of both the energy transfer, $\hbar\omega = E_1 - E_0$, and the momentum transfer, $\hbar k = \hbar(k_1 - k_0)$ during the scattering process. However, since the conventional static measurement of X-ray diffraction does not detect the $\hbar\omega$ dependence, the diffraction intensity $I[\boldsymbol{k}]$ is obtained by the integration of $S[\boldsymbol{k},\omega]$ over ω:

$$\begin{aligned} I[\mathbf{k}] &\propto \int_{-\infty}^{\infty} S[\mathbf{k},\omega] \mathrm{d}\omega \\ &= \frac{1}{2\pi}\int_{-\infty}^{\infty}\int_{-\infty}^{\infty} \sum_i \sum_j f_i^* f_j \langle \mathrm{e}^{i\mathbf{k}\mathbf{r}_i[t]} \mathrm{e}^{-i\mathbf{k}\mathbf{r}_j[0]} \rangle \mathrm{e}^{-i\omega t} \mathrm{d}t \mathrm{d}\omega \\ &= \int_{-\infty}^{\infty} \sum_i \sum_j f_i^* f_j \langle \mathrm{e}^{i\mathbf{k}\mathbf{r}_i[t]} \mathrm{e}^{-i\mathbf{k}\mathbf{r}_j[0]} \rangle \delta[t] \mathrm{d}t \\ &= \sum_i \sum_j f_i^* f_j \langle \mathrm{e}^{i\mathbf{k}\mathbf{r}_i[0]} \mathrm{e}^{-i\mathbf{k}\mathbf{r}_j[0]} \rangle \end{aligned} \qquad (2)$$

The integration in terms of ω cancels the energy dependence and hence the time dependence. This means that the scattering occurs instantaneously, and that the *momentary distribution* is the only source of the scattering intensity. In a crystal, Eq. (2) would represent the sum of the Bragg diffraction and diffuse scattering (e.g. see Appendix A in Kidera and Go 1992).

On the other hand, in Mössbauer absorption spectroscopy, owing to the high energy resolution, no integration in terms of ω is performed. Together with the incoherent nature, the cross section is written by:

$$\sigma[\mathbf{k},\omega] \propto \int \sum_j \langle e^{i\mathbf{k}\mathbf{r}_j[t]} e^{-i\mathbf{k}\mathbf{r}_j[0]} \rangle e^{-i\omega t - \Gamma|t|/2\hbar} \quad (3)$$

where $\boldsymbol{k}$ is the wave vector of gamma radiation, $\hbar\omega = E - E_a$ with E_a being the resonance energy of the nuclear transition, and Γ is the spectral width inherent in the gamma resonance (Mössbauer 1987). Equation (3) means that the absorption experiment yields information on the *temporal behavior* only for individual atoms, i.e. the Mössbauer atoms.

This difference in the nature of the observed quantities, the static distribution in X-ray diffraction and the temporal behavior of Fe in a Mössbauer spectrum, will be an important clue to understand the experimental data presented below.

Normal mode refinement

Here, let us review the idea of NM-REF in a rather informal manner (for details, see Kidera and Go 1992). The crucial point in each refinement procedure is the model for the calculation of the structure factor $F_{calc}[\boldsymbol{k}]$ [Eq. (5) below]. After calculation of the normal modes of a molecule, one is able to calculate the mean square displacements, $\langle \Delta r_j^2 \rangle_{NM}$, of each atom j by summing the contribution of each normal mode. The result can be converted into anisotropic B values.

However, the harmonic model in normal modes neglects the possibility of the conformational substates in a protein molecule. Furthermore, rigid body displacement of the whole molecule in a unit cell as described by the translation, libration, and screw (TLS) model (Schomaker and Trueblood 1968) is not taken into account. In order to obtain a model which allows a least squares fit to experimental diffraction intensities, one has to perform modifications. For simplicity, we discuss a case where only one normal mode couples to atom j (see Fig. 1). However, the molecule has two conformational substates, yielding the position $\boldsymbol{r}_\alpha$ and $\boldsymbol{r}_\beta$ for this atom. All displacements of an atom from its average position $\langle \boldsymbol{r}_j \rangle$ in the unit cell contribute to the experimental structure factors. The B values should include $\langle \Delta r_c^2 \rangle = \langle (\boldsymbol{r}_\beta - \boldsymbol{r}_\alpha)^2 \rangle$, which accounts for the contribution from the conformational substates. If the vector $\boldsymbol{r}_\beta - \boldsymbol{r}_\alpha$ has the same direction as the displacement caused by the normal mode, this can be taken into account in a good approximation by replacing the parabolas P_α and P_β describing the normal modes at atom j by a flatter parabola P_c (Fig. 1A). In this way, only the amplitude of the normal mode is changed as a free parameter to be determined by a least squares fit to the experimental data. This is called a *quasi-harmonic* approach.

A complication arises if the vector $\boldsymbol{r}_\beta - \boldsymbol{r}_\alpha$ has a different direction from the displacement caused by the normal mode (Fig. 1B). In such a case, another mode perpendicular to the original mode is required in the dynamics model. However, when the amplitudes of the two modes are used independently as the fitting parameters, we cannot reproduce the correct distribution (Fig. 1C). One has to rotate the flatter parabola P_c so that an optimal agreement with the experimental density distribution is obtained (Fig. 1D). Formally, this results in a coupling of different modes [σ_{mn} for $m \neq n$ in Eq. (5)]. In this manner, the mean square displacement, $\langle \Delta r_j^2 \rangle^X$, is determined from the fitting procedure for each atom j.

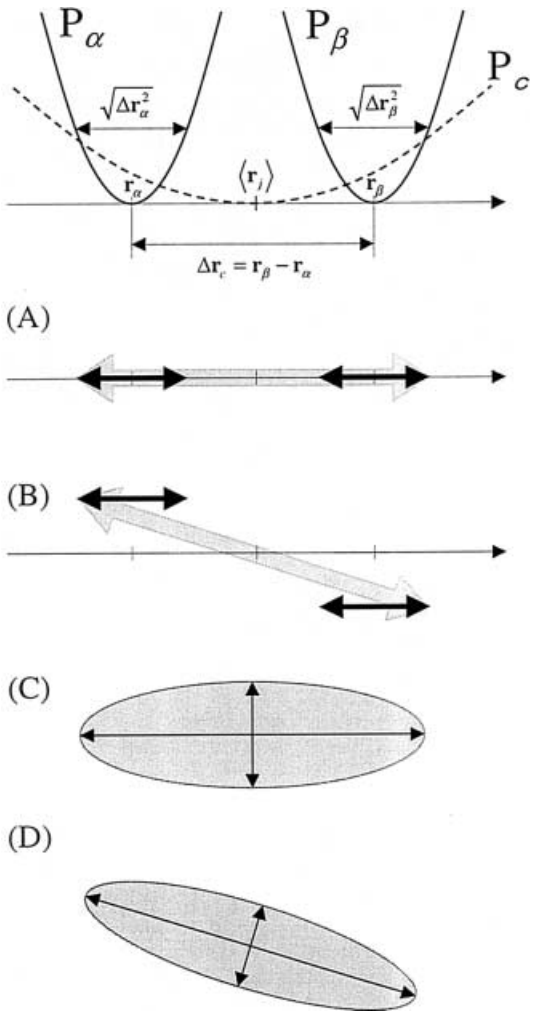

Fig. 1A–D An explanation of the principle of normal mode refinement. This figure describes how the conformational substates, P_α and P_β, are represented by a quasi-harmonic distribution, P_c. **A** A case in which the normal mode directions, Δr_α and Δr_β, coincide with the vector connecting the two average coordinates, $r_\beta - r_\alpha$. **B** A case in which the normal mode directions do not coincide with $r_\beta - r_\alpha$. **C** Thermal ellipsoid fitted to case **B**, where the amplitudes of the two modes were treated as independent variables. **D** The same as **C**, but the coupling between the two modes were considered

There still remains the problem of the large number of degrees of freedom in a protein, or the large number of free parameters in the least squares fitting. However, as explained in the Methods section, the low-frequency normal modes (less than 100) are sufficient to describe the mean square displacements of myoglobin.

The problem of the rigid body motions according to the TLS model (Schomaker and Trueblood 1968) is solved by adding an additional term to the mean square displacements. It allows the calculation of rigid body

displacements in the most general way with 21 parameters. As results of the NM-REF one obtains, for each atom j of the molecule, two anisotropic displacements:

$$\langle \Delta r_j^2 \rangle^{\mathrm{X}}_{\mathrm{total}} = \langle \Delta r_j^2 \rangle^{\mathrm{X}}_{\mathrm{internal}} + \langle \Delta r_j^2 \rangle^{\mathrm{X}}_{\mathrm{external}} \quad (4)$$

where the lower indices have the following meanings: (1) internal, displacements which change the shape of the molecule (internal displacements); (2) external, external displacement making a shift of the center of gravity and the rigid body rotation due to the TLS model; and (3) total, total (=internal+external) displacements which can be compared with the displacement obtained by the conventional B value refinement.

Methods

Here, some technical details of the NM-REF method (Kidera and Go 1992; Kidera et al. 1992) are described. The NM-REF is based on the following form of the structure factor, F_{calc}:

$$F_{\mathrm{calc}}[\mathbf{k}] = \sum_j f_j[\mathbf{k}] \exp[i\mathbf{k}\langle \mathbf{r}_j \rangle] \times \exp\left[-\frac{1}{2} \sum_{s,t=1}^{3} k_s k_t \left(\sum_{m,n=1}^{M} \Phi^{\mathrm{I}}_{jsm} \Phi^{\mathrm{I}}_{jtn} \sigma^{\mathrm{I}}_{mn} + \sum_{m,n=1}^{6} \Phi^{\mathrm{E}}_{jsm} \Phi^{\mathrm{E}}_{jtn} \sigma^{\mathrm{E}}_{mn} \right) \right] \quad (5)$$

with $\langle \mathbf{r}_j \rangle$ being the average coordinates of the atom j. In this formula, the Debye-Waller factor describing the dynamic structure of a protein is expanded in terms of normal modes. The superscripts I and E stand for internal and external normal modes, respectively; ϕ_{jsm} is the component of the m-th normal mode given theoretically by a normal mode analysis (Go et al. 1983), and σ_{mn} is covariance for the internal or external normal modes. The off-diagonal elements represent the mode coupling, or the mode rotation as explained above. The summation is over the M lowest frequency internal normal modes as well as the six external normal modes of the TLS model (Schomaker and Trueblood 1968). Therefore, after the refinement, we can decompose the dynamic structure into the internal part representing the shape-changing fluctuations and the external rigid body fluctuations. Here, M is determined by considering the balance between the number of experimental data and that of adjustable parameters. This formula for the structure factor is based on the theoretical model of protein dynamics, which states that conformational fluctuations occur mostly in the important conformational subspace spanned by a small number [M in Eq. (5)] of low-frequency normal modes (Go 1990).

The process of NM-REF consists of three steps: (1) the conventional B-factor refinement, (2) normal mode vectors, ϕ_{jsm}, are calculated as a basis set for describing the conformational fluctuations by a normal mode analysis, and (3) the coefficients for this basis set, σ_{mn}, are determined in the course of the crystallographic refinement to give the best fit to the observed diffraction data. Refinements by XPLOR (Brünger 1992) were first performed against the diffraction data listed in Table 1. In the next step, normal modes were calculated in the dihedral angle space for each set of coordinates. This step includes the regularization of bond length and bond angles to the ECEPP/2 standards (Némethy et al. 1983) and energy minimization by FEDER2 (Wako and Go 1987) using the force field parameters of ECEPP/2, and normal mode analysis, followed by a transformation of the normal mode eigenvectors of the dihedral angles to those in Cartesian coordinates. The results of the preceding steps, coordinates, B-factors of solvent atoms, and normal modes, were used in NM-REF. The model of the dynamic structure in the normal mode refinement is described by the 100 lowest frequency normal modes representing the internal fluctuations and by the six modes for the external fluctuations (the TLS model) (Schomaker and Trueblood 1968), as well as by the coupling among the 43 lowest frequency modes. Solvent atoms are described by the isotropic B-factor. The details of the method of the normal mode refinement are described in Kidera and Go (1992). The results of the refinement are summarized in Table 1.

Results and discussion

Normal mode refinements of myoglobin structure

Figure 2 demonstrates the decomposition of the total displacements $\langle \Delta r^2 \rangle^{\mathrm{X}}_{\mathrm{total}}$ into internal displacements $\langle \Delta r^2 \rangle^{\mathrm{X}}_{\mathrm{internal}}$ in the form of thermal ellipsoids of C_α

Table 1 R-factor and energy terms after the normal mode refinement

T (K)	40	115	165	260	300
Crystal data					
N_{indep}	11,936	8766	7456	13,174	15,422
Resolution (Å)	1.6–5.0	1.8–5.0	1.8–5.0	1.5–5.0	1.5–5.0
(a, b, c) (Å)	(63.70, 30.70, 34.05)	(63.80, 30.68, 34.26)	(63.81, 30.73, 34.26)	(64.35, 30.84, 34.66)	(64.52, 30.90, 34.85)
β (°)	105.65	105.66	105.65	105.77	105.80
R-factors	21.2	18.0	18.4	17.7	17.9
Intramolecular interaction energies (kcal/mol)[a]					
Bond (Å)	111 (0.015)	157 (0.019)	128 (0.017)	100 (0.015)	93 (0.015)
Angle (°)	204 (2.32)	205 (2.32)	184 (2.23)	170 (2.13)	162 (2.09)
Torsion (°)	212 (19)	223 (19)	217 (19)	190 (17)	196 (17)
Improper torsion	43 (3.2)	47 (3.4)	47 (3.4)	35 (2.9)	32 (2.7)
Lennard-Jones	–1277	–1274	–1283	–1294	–1268
Electrostatic	–4042	–3973	–3973	–4015	–4019
Hydrogen Bond	–105	–102	–94	–101	–93
Intermolecular interaction energies (kcal/mol)[a]					
Lennard-Jones	–146	–170	–160	–148	–131
Electrostatic	–159	–162	–161	–194	–206
Hydrogen Bond	–17	–16	–13	–10	–8

[a]The energy values are those of AMBER for the polar hydrogen version (Weiner et al. 1981) and those in parentheses are the deviations from the ideal values. The electrostatic energy is calculated with $\epsilon = 1$ and 8 Å cutoff

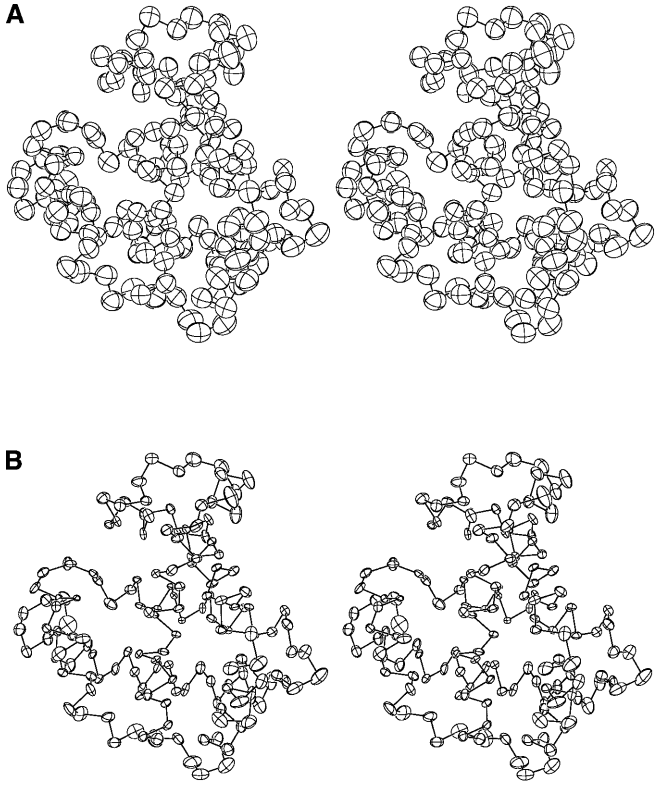

Fig. 2A, B ORTEP stereo drawing (Burnett and Johnson 1996) of thermal ellipsoids of C_α atoms of myoglobin derived from the normal mode refinement of the 300 K data. **A** Total displacements, and **B** internal displacements

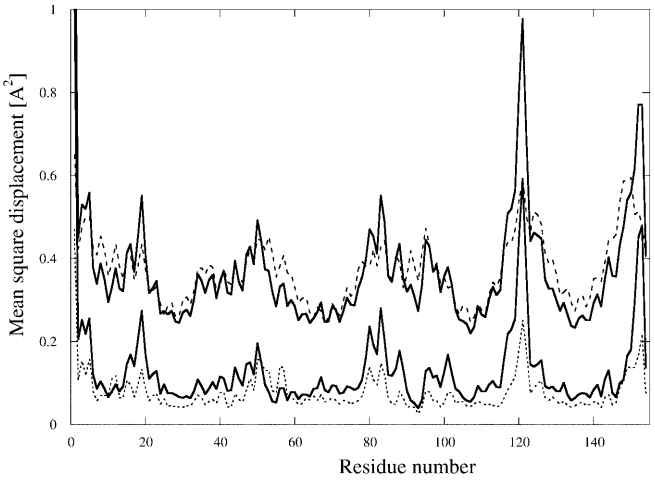

Fig. 3 Mean square displacements at 300 K averaged over the main-chain atoms in each residue. The results of normal mode refinement are given by *solid lines*. *Upper solid curve*: total displacement $\langle \Delta r^2 \rangle^{\mathrm{X}}_{\mathrm{internal}}$. *Lower solid curve*: internal displacement $\langle \Delta r^2 \rangle^{\mathrm{X}}_{\mathrm{internal}}$. For comparison: *long dashed line*: total displacement $\langle \Delta r^2 \rangle^{\mathrm{X}}_{\mathrm{TLS}}$ from a refinement using the TLS model only, with no internal mode; *short dashed line*: displacement $\langle \Delta r^2 \rangle_{\mathrm{NM}}$ obtained by normal mode analysis

atoms at 300 K, which were derived from the NM-REF. The difference between the total and the internal displacements indicates a large contribution from the external modes. The sizes of the thermal ellipsoids for the internal displacements are less than half of those for the total ones, and the anisotropy is larger in the internal displacements.

In Fig. 3, mean square displacements at 300 K are averaged over the main-chain atoms at each residue. There are four curves in Fig. 3: total displacements $\langle \Delta r^2 \rangle^{\mathrm{X}}_{\mathrm{total}}$ and internal displacements $\langle \Delta r^2 \rangle^{\mathrm{X}}_{\mathrm{internal}}$ derived from NM-REF, those calculated by another refinement using the pure TLS model with no internal mode $\langle \Delta r^2 \rangle^{\mathrm{X}}_{\mathrm{TLS}}$, and those of the normal mode analysis $\langle \Delta r^2 \rangle_{\mathrm{NM}}$. The TLS model, having only the six external modes, appears to give a similar residue dependence as $\langle \Delta r^2 \rangle^{\mathrm{X}}_{\mathrm{total}}$. However, notwithstanding the apparent agreement in Fig. 3 between the TLS and the NM-REF models, there is more than 3% difference in the *R*-factors: *R*-factor(TLS) = 21.1% and *R*-factor(NM-REF) = 17.9%. This suggests that the contributions from the internal modes are actually crucial, and the libration (L) and screw (S) modes seems to absorb some part which should be explained by the internal motions.

In Fig. 4, the temperature dependence of the internal atomic fluctuations is illustrated by the thermal ellipsoids of the heme group as well as the proximal histidine (His93). The gradual shrinking of the thermal ellipsoids on lowering the temperature is clearly seen in this figure. The temperature dependence is not necessarily uniform at all atoms. Particularly, the side-chain atoms of the heme group remain to be distributed even at 40 K. This should be attributed to the static disorder.

Figure 5A compares the mean square displacements at the Fe position obtained by different experimental techniques and different evaluation procedures. The thick solid line gives the mean square displacement obtained by a normal mode analysis, $\langle \Delta r^2 \rangle_{\mathrm{NM}}$. Below the dynamical transition temperature T_c ($\sim$180 K), the mean square displacements obtained by Mössbauer spectroscopy $\langle \Delta r^2 \rangle^{\gamma}$ are well explained by the normal mode curve. However, above T_c, the $\langle \Delta r^2 \rangle^{\gamma}$ values increase more strongly with temperature than predicted by the normal modes. Total and internal mean square displacements, $\langle \Delta r^2 \rangle^{\mathrm{X}}_{\mathrm{total}}$ and $\langle \Delta r^2 \rangle^{\mathrm{X}}_{\mathrm{internal}}$, obtained from NM-REF are shown as open squares and filled squares, respectively. The temperature dependence of $\langle \Delta r^2 \rangle^{\mathrm{X}}_{\mathrm{internal}}$ can well be fitted by linear regression curves. The values of $\langle \Delta r^2 \rangle^{\mathrm{X}}_{\mathrm{internal}}$ are larger than those of $\langle \Delta r^2 \rangle_{\mathrm{NM}}$. However, the rate of increase with temperature is very similar. The analogous temperature dependence can be seen also in the average of all non-hydrogen atoms and the average of the main-chain atoms of myoglobin. Again very similar slopes for $\langle \Delta r^2 \rangle_{\mathrm{NM}}$ and $\langle \Delta r^2 \rangle^{\mathrm{X}}_{\mathrm{internal}}$ were found, as shown in Fig. 5B. In summary, the internal average mean square displacements show linear temperature dependencies as:

$$\langle \Delta r^2 \rangle^{\mathrm{X}}_{\mathrm{internal}} = \alpha T + \beta \qquad (6)$$

throughout the temperature range measured here.

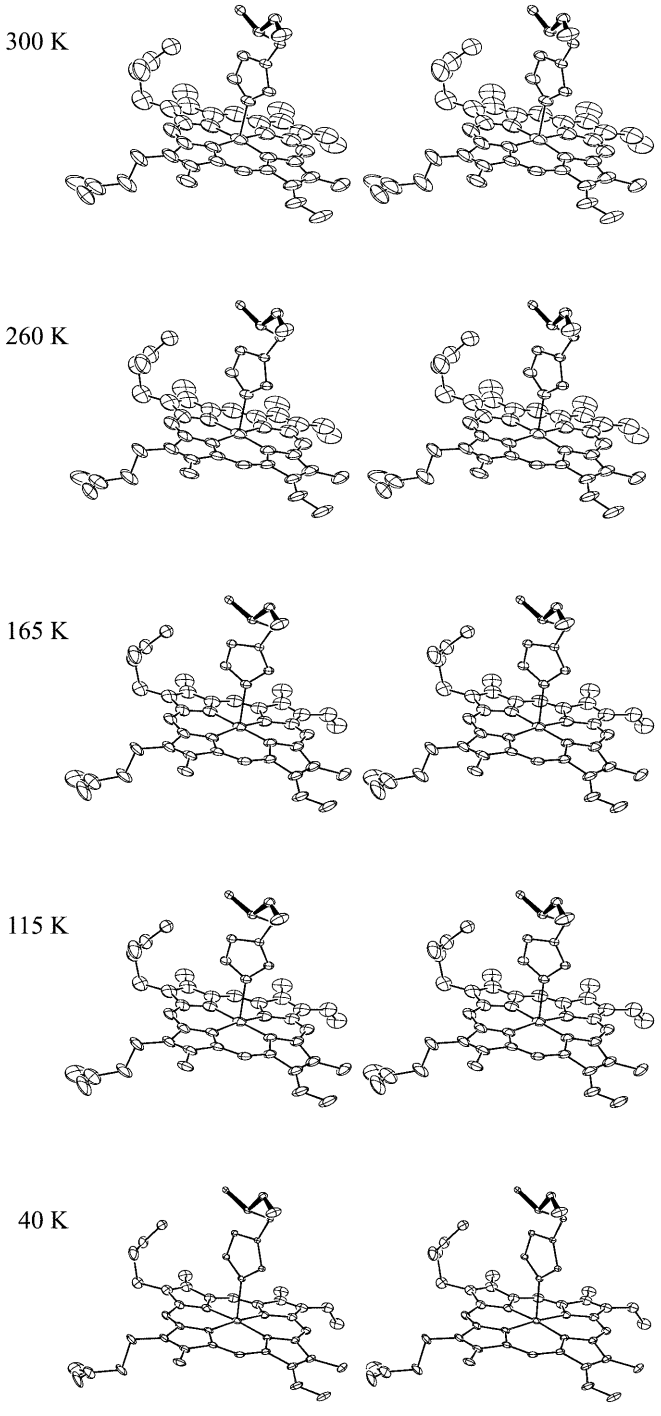

Fig. 4 ORTEP stereo drawing (Burnett and Johnson 1996) of thermal ellipsoids of heme and the proximal histidine (His93). These are the internal displacements determined at each temperature by the normal mode refinement

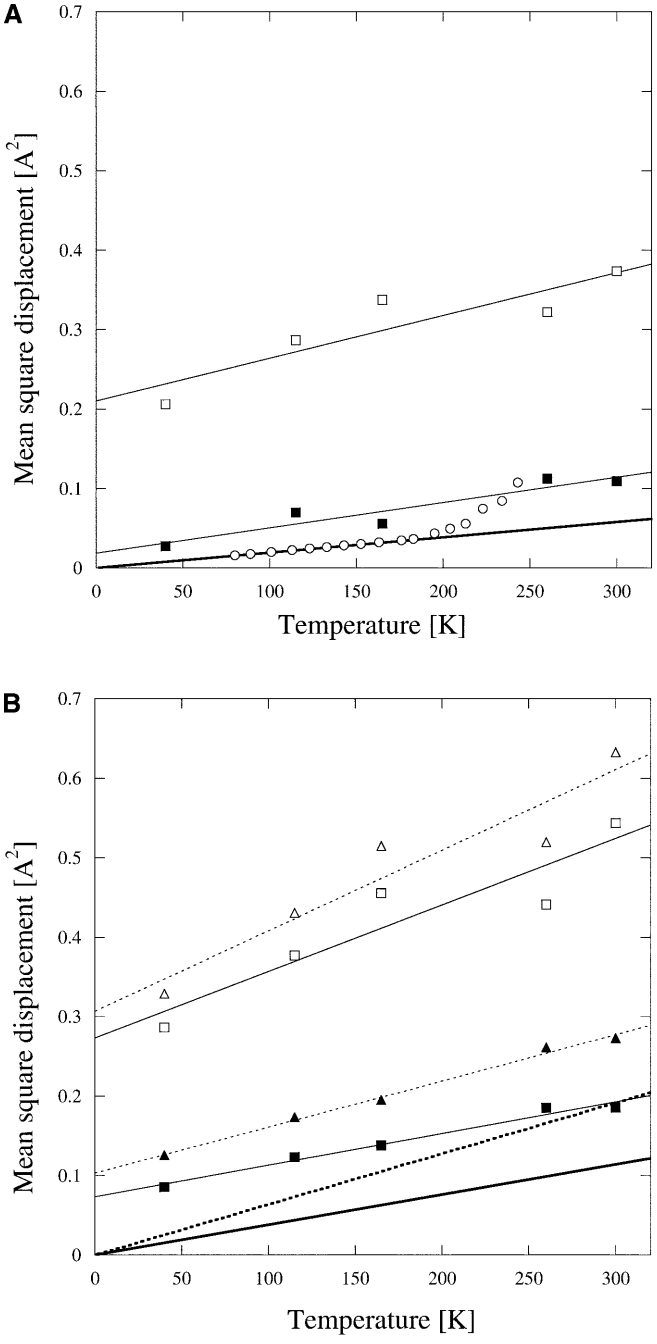

Fig. 5A, B Temperature dependence of mean square displacements. **A** Displacements of the iron: *circles*: $\langle \Delta r^2 \rangle^{\gamma}$ values derived from Mössbauer absorption experiments; *thick line*: calculated from normal modes; *open squares*: $\langle \Delta r^2 \rangle^{X}_{\text{total}}$ values, derived from the X-ray refinement, which correspond to the isotropic *B*-values; *filled squares*: normal mode refinement. The *lines* give linear regressions. **B** The average values for all non-hydrogen atoms (*triangles*) and for main-chain atoms (*squares*) derived from the X-ray refinement; *open symbols*: total displacements, $\langle \Delta r^2 \rangle^{X}_{\text{total}}$, corresponding to the isotropic *B*-values; *filled symbols* are for the internal displacements, $\langle \Delta r^2 \rangle^{X}_{\text{internal}}$, separated from $\langle \Delta r^2 \rangle^{X}_{\text{total}}$ by the normal mode refinement. The *thick line* represents the temperature dependence predicted by a normal mode analysis. The *thin lines* are the linear regression curves

More explicitly, Fig. 6A plots the linear regression coefficient, α in Eq. (6), averaged over the main-chain atoms at each residue. A high correlation coefficient (0.72) and a small root-mean-square difference (0.00021 Å^2/K) from those calculated by the normal mode analysis indicate that the temperature dependence of $\langle \Delta r^2 \rangle^{X}_{\text{internal}}$ is practically the same at every residue.

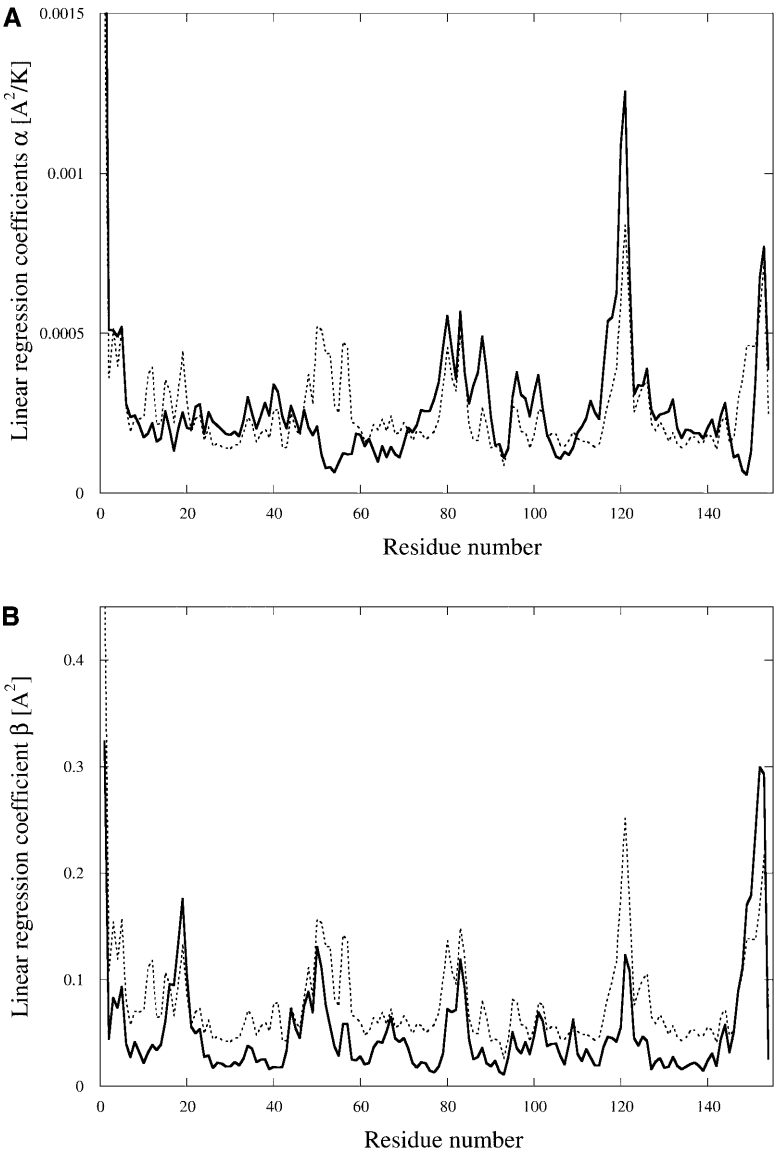

Fig. 6A, B The linear regression coefficients (the values of α and β in $\langle \Delta r^2 \rangle^{X}_{internal} = \alpha T + ß$) averaged over the main-chain atoms at each residue are plotted against residue number. Here, the residue 154 is assigned to the heme group. **A** The values of α (*thick solid line*) are compared with those calculated by a normal mode analysis (*thin broken line*). The slope of $\langle \Delta r^2 \rangle^{X}_{internal}$ for Fe shown in Fig. 5A is 0.00032 Å^2/K. **B** The values of β (*thick solid line*) are compared with mean square displacements of the normal mode analysis at 300 K. The extrapolated value of $\langle \Delta r^2 \rangle^{X}_{internal}$ for Fe at 0 K shown in Fig. 5A is 0.0185 Å^2

However, there can be seen some discrepancies in the plot, particularly at the D helix (residues 51–57), where the values for α of $\langle \Delta r^2 \rangle^{X}_{internal}$ are much smaller than those for $\langle \Delta r^2 \rangle_{NM}$. This discrepancy can be attributed to a sulfate ion connecting two molecules in the crystal, at residues 50–52 in one molecule and 58–60 in another molecule (compare Fig. 7). It is expected that the strong coordination by the sulfate ion leads to suppression of the fluctuation at the D helix. Therefore, the values of $\langle \Delta r^2 \rangle_{NM}$, which were calculated without considering the interactions with the sulfate ion, should have an overestimation, as do the α values.

The agreement in the values of α can be easily understood if one takes into account that a protein molecule can exist in a large number of conformational substates. The distribution of these substates occupied at a certain temperature may be characterized by the mean square displacement $\langle \Delta r_c^2 \rangle$ defined in Fig. 1. Therefore, the result of the normal mode refinement should be represented by convolution of normal mode motions and a set of conformational substates, i.e.:

$$\langle \Delta r^2 \rangle^{X}_{internal} = \langle \Delta r^2 \rangle_{NM} + \langle \Delta r_c^2 \rangle \quad (7)$$

Let us now discuss the temperature dependence. Mean square displacements obtained from normal modes increase linearly with temperature by definition, since a harmonic approximation is used. If the temperature increase of $\langle \Delta r^2 \rangle^{X}_{internal}$ has a similar slope as $\langle \Delta r^2 \rangle_{NM}$, this indicates that $\langle \Delta r_c^2 \rangle$ is practically temperature independent. Here, one has to remember that X-ray diffraction involves pair correlation given at a certain instance. The displacement from the average coordinates enter the Debye-Waller factor irrespective of any time dependence. This clearly shows that it makes no difference if, in the ensemble of protein molecules under investigation, each molecule is trapped in a particular conformational substate from a distribution of

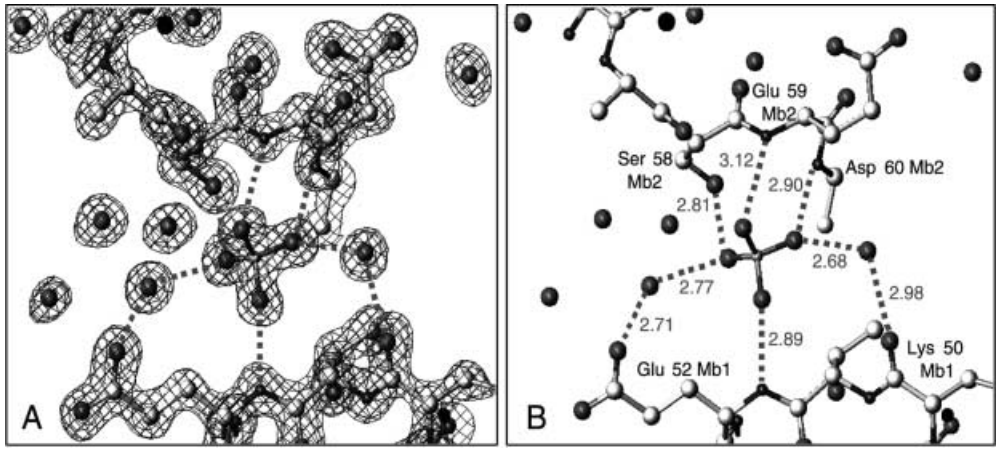

Fig. 7 **A** The electron density map around a sulfate ion connecting two molecules where the contour is for the 1.5σ level; **B** the hydrogen-bond network of the same region

states or if it is jumping between different substates. Only if the set of the substates increases would the slope of $\langle \Delta r^2 \rangle^{X}_{\text{internal}}$ also increase. Then, a temperature independence of $\langle \Delta r_c^2 \rangle$ means that in myoglobin crystals practically the same conformational substates are occupied in the temperature range considered. Comparing Eqs. (6) and (7), we find the correspondence $\langle \Delta r^2 \rangle_{\text{NM}} = \alpha T$ and $\langle \Delta r_c^2 \rangle = \beta$ in this approach.

These observations are closely related to the way of cooling the crystal below T_c. If the crystal were cooled down slowly enough to make protein molecules attain the equilibrium state, the number of substates occupied by the molecules should decrease on lowering the temperature. However, such a cooling method may destroy the crystal owing to the formation of an ice phase at around 200 K. In this study, to prevent ice formation, the crystal was subject to shock freezing at liquid propane temperature (Parak et al. 1977). This process may be so rapid that molecules do not have enough time for relaxing to more stable substates before freezing. The 260 K data were taken by flash cooling, which is a much slower process, allowing redistribution of the substates. However, there is still no indication of change in $\langle \Delta r_c^2 \rangle$. This implies that within the limit of the experimental accuracy, the set of available substates at 260 K is substantially the same as those at 300 K.

When we look at the total displacement shown in Fig. 5B, it is found that there is a rather large decrease in $\langle \Delta r^2 \rangle^{X}_{\text{total}}$ on reducing the temperature from 300 K to 260 K, which is not seen in the $\langle \Delta r^2 \rangle^{X}_{\text{internal}}$ values. It suggests that the redistribution of the substates occurs mostly in the rigid-body motions to change the position and orientation of the molecules in the crystal.

The average values of the regression coefficient β in Eq. (6), i.e. $\langle \Delta r_c^2 \rangle$, for the main-chain atoms are plotted against the residue number in Fig. 6B. It is noticed that the values of β again have a high correlation coefficient (0.74) with those predicted by the normal mode analysis. This means that the width of the distribution of the substates for each locus is proportional to $\langle \Delta r^2 \rangle_{\text{NM}}$. In other words, there are many substates along a mode having a large amplitude. This observation is consistent with the result of an analysis of a molecular dynamics trajectory (Kitao et al. 1998), where the substates were found to distribute along the conformational subspace spanned by low-frequency normal modes.

As discussed just above, the similarity of the slopes of $\langle \Delta r^2 \rangle^{X}_{\text{internal}}$ and $\langle \Delta r^2 \rangle_{\text{NM}}$ with temperature is a consequence of the rapid freezing of the crystals. However, one has to have in mind that this rapid freezing is only a limiting case. Analyzing in detail the slopes of $\langle \Delta r^2 \rangle^{X}_{\text{internal}}$ for the different residues shows that some of the α values for $\langle \Delta r^2 \rangle^{X}_{\text{internal}}$ are larger than the corresponding predictions of the normal mode. Therefore, on lowering the temperature, some relaxation to the more stable conformational substates is still present. It should be mentioned in passing that structural relaxations have been found below T_c but on a very large time scale of days and more. This is clearly demonstrated by the relaxations of low-spin Fe(II)H_2O-ligated myoglobin into deoxymyoglobin (Prusakov et al. 1995).

Mössbauer spectroscopy

Mössbauer spectra of myoglobin crystals were measured over a large temperature range, as shown in Fig. 5A. The mean square displacement of the iron, $\langle \Delta r^2 \rangle^{\gamma}$, is determined from the Lamb Mössbauer factor f as given in:

$$f = \exp\left[-k^2 \frac{\langle \Delta r^2 \rangle^{\gamma}}{3}\right] \tag{8}$$

where $k = 2\pi/\lambda$ and $\lambda = 0.86$ Å for ^{57}Fe. The Lamb Mössbauer factor f depends only on dynamical displacements of the iron, which occur on a time scale faster than 140 ns. The Lamb Mössbauer factor f is proportional to the logarithm of the absorption area of the Mössbauer spectrum, which is determined by a least squares fit of a doublet of Lorentzians. At temperatures above T_c ($\sim$180 K), the Mössbauer spectra can no longer be fitted by two Lorentzians. The spectrum of CO-ligated myoglobin crystals measured at $T = 243$ K is shown in

Fig. 8 as an example. In addition to the doublet of Lorentzians, broad lines are necessary in order to give a good representation of the experimental data. At temperatures where the broad lines occur, the mean square displacements calculated from the area of the narrow Lorentzians increase more than linearly with temperature (see Fig. 5A). In Mössbauer spectroscopy, the appearance of narrow Lorentzians together with broad lines indicate diffusive motions limited in space. The spectra have been described by models like jump diffusion with a Cole-Davidson jump time distribution (Chang et al. 1996) or by a Brownian oscillator (Knapp et al. 1982). These bound diffusions are essential for the fluctuations of the protein molecules between conformational substates. However, this does not exclude other processes on a much longer time scale present even below T_c. In Fig. 8, we used the following equation for the transmission spectrum τ:

$$\tau = f_s \left\{ 1 - \text{const} \times e^{-\frac{k^2}{3}(\langle r_v^2\rangle + \langle \Delta r_t^2\rangle)} \sum_{l=1}^{2} \sum_{N=0}^{\infty} \frac{\left(\frac{k^2}{3}\langle \Delta r_t^2\rangle\right)^N}{N!} \times \frac{\frac{\Gamma_a+\Gamma_s}{2} + N\alpha_t}{\left(E_{al} - E_s\left(1-\frac{v}{c}\right)\right)^2 + \left(\frac{\Gamma_a+\Gamma_s}{2} + N\alpha_t\right)^2} \right\} \quad (9)$$

The mean square displacement is determined by $\langle \Delta r_v^2 \rangle$, coming from modes of motions which are present at low temperatures, and which we extrapolate into the high-temperature regime, and by $\langle \Delta r_t^2 \rangle$, which comes from the bound diffusion present only above T_c. The parameter α_t depends on the ratio of the damping and backdriving forces and determines the width of the additional broad lines. Trivial parameters are the energy center of the resonance line and the energy width in the absorber and the source, E_a, Γ_a, E_s, and Γ_s, respectively;

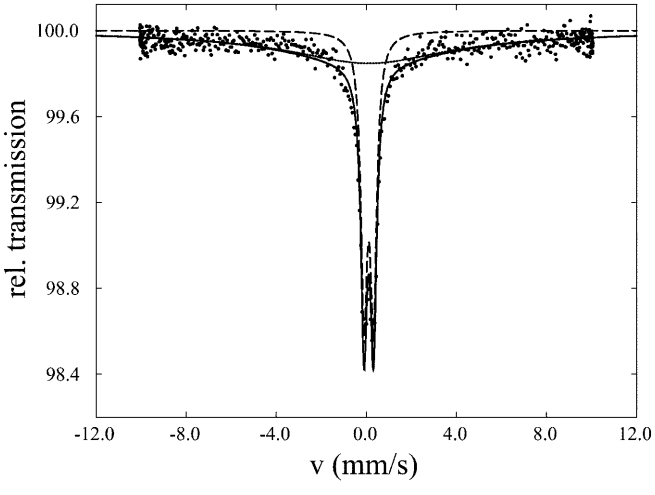

Fig. 8 Mössbauer spectrum of MbCO crystals at 243 K. *Dashed line*: quadrupole doublet of Lorentzians; *dotted line*: broad additional line which indicates quasi-diffusive processes; *solid line*: least squares fit according to Eq. (9)

f_s is the Lamb Mössbauer factor of the source, v/c gives the ratio of the velocity of the Mössbauer drive with respect to the velocity of light, and the index l takes into account the quadrupole splitting. It is important to note that above T_c two processes occur. Firstly, the area of the narrow Lorentzians continues to decrease with temperature according to Eq. (8), with $\langle \Delta r^2 \rangle^{\gamma} = \langle \Delta r_v^2 \rangle$.

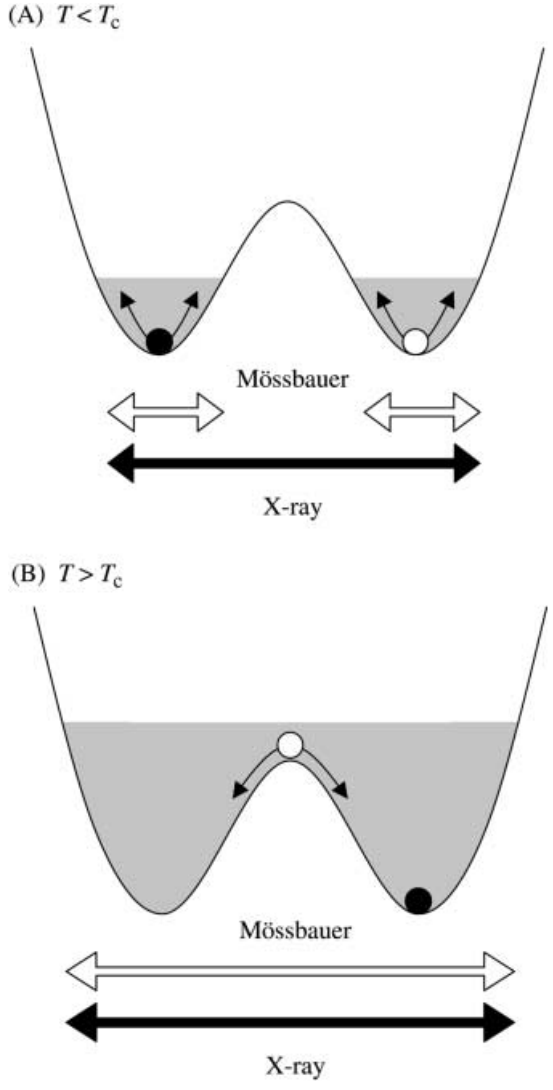

Fig. 9A, B A schematic explanation of the difference in the temperature dependence of myoglobin dynamics between X-ray diffraction and Mössbauer absorption spectroscopy. Well below T_c (ca. 180 K), each molecule in the crystal is trapped in a basin of a conformational substate. X-ray diffraction measures the static distribution whose mean square displacement is $\langle \Delta r^2 \rangle^{X}_{\text{internal}} = \langle \Delta r^2 \rangle_{NM} + \langle \Delta r_c^2 \rangle$ where $\langle \Delta r_c^2 \rangle$ is temperature independent, whereas Mössbauer detects the temporal behavior of the Fe atom whose mean square displacement is $\langle \Delta r^2 \rangle^{\gamma} = \langle \Delta r^2 \rangle_{NM}$. Well above T_c, molecules cross over the potential barrier to reach another substate. The increment of displacement that X-ray diffraction observes is only the linear increase in $\langle \Delta r^2 \rangle_{NM}$, while Mössbauer now counts the contribution from $\langle \Delta r_c^2 \rangle$. The figure here is shown for a simplified case in which the vector connecting the average coordinates of two substates are in parallel to the incident Mössbauer beam. In this case only, the energy barrier occurs in the depicted one-dimensional space

Assuming that the normal mode vibrations give rise to $\langle \Delta r_v^2 \rangle$, this means that essentially they are still present at room temperature. Secondly, the more than linear increase of the total $\langle \Delta r^2 \rangle^\gamma$ because of $\langle \Delta r_t^2 \rangle$ can then be treated as an additive effect. It also has to be mentioned that jumps between conformational substates usually occur along a path not directly connecting the substates because of the necessity of the structural rearrangement of the whole molecule in a high-dimensional conformational space. The $\langle \Delta r_v^2 \rangle$, and the $\langle \Delta r_t^2 \rangle$, values give only projections in one direction defined by the incoming Mössbauer radiation.

How does this picture of the Mössbauer spectroscopy fit with the results of the normal mode refinement? As schematically summarized in Fig. 9, the difference in the mean square displacement shown in Fig. 5A originates from the special physical nature of X-ray diffraction and Mössbauer absorption spectroscopy. The distributions of the conformational substates, $\langle \Delta r_c^2 \rangle$, have an influence on X-ray diffraction, yielding a positive value of β in Eq. (6), but do not affect a Mössbauer spectrum, yielding zero value of β. Below T_c, the gradient values of α, determined in X-ray diffraction and Mössbauer spectroscopy, are both the same as those of the normal mode analysis, indicating normal mode vibration within a substate. Above T_c in a narrow temperature range, molecules start to explore different conformational substates. This is directly reflected in the Mössbauer spectrum to give the strong increase in the $\langle \Delta r^2 \rangle^\gamma$ value, indicating a dynamical transition. On the other hand, the dynamical transition cannot be detected clearly in X-ray diffraction, because of its coherent nature and the temperature independent distribution, $\langle \Delta r_c^2 \rangle$, of the conformational substates.

Above $\sim$230 K, $\langle \Delta r^2 \rangle^\gamma$ becomes larger than $\langle \Delta r^2 \rangle^X{}_{\text{internal}}$, and may finally approach $\langle \Delta r^2 \rangle^X{}_{\text{total}}$, because Mössbauer spectroscopy does not distinguish the internal fluctuations from the external ones. Let us consider again the good agreement between $\langle \Delta r^2 \rangle^\gamma$ and $\langle \Delta r^2 \rangle_{NM}$ below T_c. Although the $\langle \Delta r^2 \rangle^\gamma$ values contain both the internal and external (TLS) contributions, $\langle \Delta r^2 \rangle_{NM}$ reflects purely the internal motions. This implies that the external motions are prohibited below T_c, probably owing to the hydrogen-bond network of solvent water molecules surrounding myoglobin. Above T_c, such a network starts to melt down to allow certain quasi-diffusive rigid-body motions in myoglobin molecules. However, it should be mentioned that $\langle \Delta r_t^2 \rangle$ does not solely originate from the diffusive rigid-body motions. Above T_c, there must be both internal and external contributions to $\langle \Delta r_t^2 \rangle$. The static distribution derived from X-ray diffraction cannot distinguish the types of motions, whether vibrational or diffusive.

Acknowledgements This work was supported by a grant from the International Scientific Research Program, Joint Research, from the Ministry of Education, Japan, and the Deutsche Forschungsgemeinschaft SFB 533. We thank K. Achterhold for helpful discussions.

References

Brünger AT (1992) X-PLOR, version 3.1: a system for X-ray crystallography and NMR. Yale University, New Haven

Burnett MN, Johnson CK (1996) ORTEP-III: Oak Ridge thermal ellipsoid plot program for crystal structure illustrations. Oak Ridge National Laboratory, Tenn., report ORNL-6895

Chang I, Hartmann H, Krupyanskii Yu, Zharikov A, Parak F (1996) Dielectric relaxation models applied to the dynamics of myoglobin as determined by Mössbauer spectroscopy. Chem Phys 212:221–229

Ferrand M, Dianoux AJ, Petry W, Zaccai G (1993) Thermal motions and function of bacteriorhodopsin in purple membranes: effects of temperature and hydration studied by neutron scattering. Proc Natl Acad Sci USA 90:9668–9672

Doster W, Cusack S, Petry W (1989) Dynamic transition of myoglobin revealed by inelastic neutron scattering. Nature 337:754–756

Go N (1990) A theorem on amplitudes of thermal atomic fluctuations in large molecules assuming specific conformations calculated by normal mode analysis. Biophys Chem 35:105–112

Go N, Noguti T, Nishikawa T (1983) Dynamics of a small globular protein in terms of low-frequency vibrational modes. Proc Natl Acad Sci USA 80:3696–3700

Green JL, Fan J, Angell CA (1994) The protein-glass analogy: some insights from homopeptide comparisons. J Phys Chem 98:13780–13790

Kidera A, Go N (1992) Normal mode refinement: crystallographic refinement of protein dynamic structure I. Theory and test by simulated diffraction data. J Mol Biol 225:457–475

Kidera A, Inaka K, Matsushima M, Go N (1992) Normal mode refinement: crystallographic refinement of protein dynamic structure II. Application to human lysozyme. J Mol Biol 225:477–486

Kitao A, Hayward S, Go N (1998) Energy landscape of a native protein: jumping-among-minima model. Proteins 33:496–517

Knapp EW, Fischer SF, Parak F (1982) Protein dynamics from Mössbauer spectra. The temperature dependence. J Phys Chem 86:5042–5047

Krupyanskii YF, Parak F, Goldanskii VI, Mössbauer RL, Gaubmann EE, Engelmann H, Suzdaley IP (1982) Investigation of large intramolecular movements within metmyoglobin by Rayleigh scattering of Mössbauer radiation (RSMR). Z Naturforsch C 37:57–62

Mössbauer RL (1987) Gamma-resonance and X-ray investigations of slow motions in macromolecular systems. Hyperfine Interact 33:199–222

Némethy G, Pottle MS, Scheraga HA (1983) Energy parameters in polypeptides. 9. Updating of geometrical parameters, nonbonded interactions, and hydrogen bond interactions for the naturally occurring amino acids. J Phys Chem 87:1883–1887

Nienhaus GU, Parak F (1986) Rayleigh scattering of Mössbauer radiation on metmyoglobin. Hyperfine Interact 29:1451–1454

Ostermann A, Waschipky R, Parak FG, Nienhaus GU (2000) Ligand binding and conformational motions in myoglobin. Nature 404:205–208

Parak F, Formanek H (1971) Untersuchung des Schwingungsanrteils und des Kristallgitterfehleranteils des Temperaturfaktors in Myoglobin durch Vergleich von Mössbauerabsorptionsmessungen mit Röntgenstrukturdaten. Acta Crystallogr Sect A 27:573–578

Parak F, Knapp EW (1984) A consistent picture of protein dynamics. Proc Natl Acad Sci USA 81:7088–7092

Parak F, Thomanek UF, Bade D, Wintergerst B (1977) The orientation of the electric field gradient tensor in CO-liganded myoglobin. Z Naturforsch C 32:507–512

Parak F, Knapp EW, Kucheida D (1982) Protein dynamics Mössbauer spectroscopy on deoxymyoglobin crystals. J Mol Biol 161:177–194

Parak F, Hartmann H, Aumann KD, Reuscher H, Rennekamp G, Bartunik H, Steigemann W (1987) Low temperature X-ray investigation of structural distributions in myoglobin. Eur Biophys J 15:237–249

Parak F, Ostermann A, Gassmann A, Scherk C, Chong S-H, Kidera A, Go N (1999) Biomolecules: fluctuations and relaxations. In: Frauenfelder H, Hummer G, García R (eds) Biological Physics, 3rd Int. Symposium Santa Fe 1998. Am Inst Phys, pp 117–123

Prusakov VE, Steyer J, Parak FG (1995) Mössbauer spectroscopy on nonequilibrium states of myoglobin: a study of r-t relaxation. Biophys J 68:2524–2530

Rasmussen BF, Stock AM, Ringe D, Petsko GA (1992) Crystalline ribonuclease A loses function below the dynamical transition at 220 K. Nature 357:423–424

Schomaker V, Trueblood KN (1968) On the rigid body motion of molecules in crystals. Acta Crystallogr Sect B 24:63–76

Wako H, Go N (1987) Algorithm for rapid calculation of Hessian of conformational energy function of proteins by supercomputer. J Comput Chem 8:625–635

Weiner PK, Kollman PA (1981) AMBER: assisted model building with energy refinement. A general program for modeling molecules and their interactions. J Comput Chem 2:287–303